Iranian Journal of Oil & Gas Science and Technology, Vol. 2 (2013), No. 1, pp. 57-70
http://ijogst.put.ac.ir

Effect of Water/Alkoxide Molar Ratio on the Synthesis Process and Electrochemical Behavior of Yttria-doped Zirconia Sol-gel Films

S. Rezaee[1], Gh. R. Rashed[1*], and M. A. Golozar[2]

[1] Department of Technical Inspection Engineering, Petroleum University of Technology, Abadan, Iran
[2] Department of Material Science Engineering, Isfahan University of Technology, Isfahan, Iran

Abstract

The aim of this work is to synthesize and investigate the performance of yttria-doped zirconia sol-gel coatings in the chemical corrosion prevention of zircaloy-4 (zirconium alloy) in a 1 N H_2SO_4 environment. The influence of four different molar ratios of water to alkoxide, namely 1, 4, 12, and 20, on the coating quality and its corrosion prevention performance was investigated. Differential thermal analysis and thermogravimetric analysis (DTA-TG) revealed the coating formation process. Surface morphology was examined using scanning electron microscopy (SEM). Microscopic features were obtained by employing energy dispersive spectroscopy (EDX) and X-ray diffraction (XRD). Wet corrosion performance was evaluated by using potentiodynamic polarization and electrochemical impedance spectroscopy (EIS) techniques. The EDX results approved that the amount of the yttria doped in zirconia was about 8 wt.%. The XRD results showed that the crystallization of zirconia started near 400 °C. The SEM results showed that denser cracks were formed at a water/alkoxide molar ratio of 4. The electrochemical tests revealed that, as the molar ratio of water to alkoxide was increased beyond 4, the coating quality was damaged and the best protection performance was achieved at a water/alkoxide molar ratio of 4.

Keywords: Sol-gel, Yttria-stabilized Zirconia (YSZ) Coating, Hydrolysis, Crack-free Coating, Corrosion Performance, Yttria-doped Zirconia Coating

1. Introduction

Zirconium and its alloys are materials with a very versatile structure used in nuclear reactors, chemical engineering, and lately in biomedical applications (Xue et al., 2010; Peng et al., 2005; Chen et al., 2006; Shoesmith et al., 2011; Peng et al., 2005). They have been chosen for these applications because of their combination of a low thermal neutron capture cross-section, favorable mechanical properties, and good corrosion resistance. However, they are subject to corrosion and erosion (Peng et al., 2004; Peng et al., 2003; Stojilovic et al., 2005; Sanchez et al., 2011; Kim et al., 2010). To improve its surface performance, while retaining its balk properties, a proper surface treatment such as ion implantation, plasma spray, anodization, etc. might be an effective method according to the previous works (Xue et al., 2010; Peng et al., 2005; Peng et al., 2004; Peng et al., 2003; Sanchez et al., 2011; Peng et al., 2005). Sol-gel method is another surface modification technique which has been extensively used for many years because it possesses a number of advantages over other techniques. They include forming inorganic structures at relatively low temperatures, producing thin homogeneous inorganic films on

* Corresponding Author:
Email: g.rashed@put.ac.ir

large scales, controlling the precursor solution stoichiometry effectively, forming porous films and homogeneous multi-component oxide films, obtaining higher purity from raw materials, controlling film thickness, and being a cost effective method (Lopez et al.; 2011; Voevodin et al., 2001; Kiruthika et al., 2010; Fedrizzi et al., 2001; Liu et al., 2002). This method is widely used for producing ceramic coatings like silica (Lopez et al., 2011), Al_2O_3 (Zhen-lin et al., 2010), zirconate film (Voevodin et al., 2001), cerium-nitrate-doped ZrO_2 (Paussa et al., 2012), yttria-stabilized zirconia (YSZ) (Crespo et al., 2009), SiO_2-ZrO_2 (Kiruthika et al., 2010), ZrO_2 (Li et al., 2001; Carrion et al., 2010), TiO_2-SiO_2 (Jokinen et al., 1998), etc. Among all the ceramic coatings derived from the sol-gel method, the YSZ coatings have widely been used in recent years because of their more efficient anti-corrosion ability, thermal protection, optical properties, easier sol preparation, good erosion resistance accompanied by a toughened strength, and their thermal expansion coefficient which is close to many metals and alloys (Kiruthika et al., 2010; Paussa et al., 2012; Crespo et al., 2009; Li et al., 2001; Carrion et al., 2009; Neto et al., 1994). In gel-derived coatings, the intrinsic stress generation during the heating-up stage causes the crack formation, which is the main problem especially in films thicker than 0.1 μm (Fedrizzi et al.; 2001; Sakka, 2004; Nouri et al., 2012). There are some controllable factors which can influence crack-free film production; some of them have been investigated by other researchers. Lopez found that the corrosion resistance was improved by increasing the number of deposited silica layers because they became free of cracks and porosities (Lopez at al., 2011). It was also found that denser and more crack-free zirconia and silica films were formed at higher temperatures because of the removal of organic substances (Crespo et al., 2009; Li et al., 2008; Lopez et al., 2011); this also helps to increase the anticorrosive properties of the coatings. Baron concluded that the basic catalysts were more effective in crack-free film production compared with acidic catalysts and denser films were produced in more diluted sols (Baron et al., 2011). Ugas-Carrion revealed that by using an optimum acetylacetone concentration as a complexing agent the porosity and defects of zirconia coatings could be reduced even at low temperatures (Carrion et al., 2009). The current study concentrates on the synthesis of 8 wt.% yttria-stabilized zirconia sol and sol-gel dip coatings using a zirconium propoxide/yttrium chloride/acetylacetone/water system in ethanol as a solvent. The bare zircaloy-4 (zirconium alloy) substrate is considered as a reference. This work describes how yttria-stabilized zirconia coating can improve the corrosion resistance of zircaloy-4. Also, the influence of different ratios of water to alkoxide on the coating quality and its corrosion prevention performance is investigated.

2. Materials and methods

2.1. Sol and coating preparation

The samples of zircaloy-4 were cut in rectangular sheets with the size of 20 mm×10 mm having a thickness of 1 mm. The chemical composition of the zircaloy-4 is represented in Table 1. They were mechanically polished using sand papers (120- to 600-grade papers), cleaned in acetone, and then dried under air pressure. The sol of ZrO_2-8 wt.%-Y_2O_3 was obtained using zirconium (IV) propoxide (70 wt.% in 1-propanol), acetylacetone as a stabilizing agent, and water at the molar ratios of 1:3:h respectively. The molar ratio of water to /alkoxide varied from 1 to 20 having the values of 1, 4, 12, and 20. Yttrium (III) chloride (99.99% anhydrous powder) was used as a stabilizing agent and ethanol as the solvent.

Acetylacetone was added to zirconium propoxide to control the reactions; a proper quantity of ethanol was well mixed with the previous solution using a magnetic stirrer. Then, the precursor solution was gradually added to a proper amount of water while stirring continued. Finally, yttrium (III) chloride was added to the solution under continuous stirring. After about 30 minutes, a yellow, stable, and

transparent precursor sol was obtained. Zirconium concentration in the final solution was 0.15 M. No precipitate was observed even after 6 months. The zircaloy-4 substrates were then coated by the dip coating technique with a controlled immersion and withdrawal speed of 1 $mm.s^{-1}$; the immersion time interval was 3 minutes. After each of three depositions, the coatings were treated up to 300 °C at a heating rate of 10 $°C.min^{-1}$. Lastly, they were heated up to 700 °C, and then were thermally annealed at this temperature for 1 hour to remove water and organic compounds and get a dense film.

Table 1
Elemental composition of zircaloy-4

Element	Sn	Fe	Cr	Ni	Zr
Percent (wt. %)	1.55	0.15	0.1	0.05	Balance

(Fe + Cr + Ni = 0.3 wt.%)

2.2. Characterization

The morphology of the films before electrochemical measurements was studied by a scanning electron microscope (SEM, VEGA, TESCAN-LMU). The chemical composition was evaluated by energy dispersive X-ray spectroscopy (EDX). X-ray diffraction (XRD) (Bruker, D8ADVANCE, Germany; X-Ray Tube Anode: Cu, Wavelength: 1.5406 Å (Cu K_α)) was used to determine the chemical composition and the crystalline phase structure transformation of the dried gel powder at 3 different temperatures of 150 °C, 400 °C, and 700 °C. The crystallite size of the films was determined from the half-height width of the XRD peak using Scherrer equation. The process pathways such as water or organic substance evaporation and phase transitions were studied by the thermal analysis of the samples heated from room temperature to 800 °C in air atmosphere at a heating rate of 10 $°C.min^{-1}$ using TG-DTA (Model L81, 1750, Linseis, Germany). Open circuit potential (OCP), electrochemical impedance spectroscopy (EIS), and potentiodynamic polarization tests were carried out to evaluate the effect of the YSZ coatings on the corrosion prevention performance of zircaloy-4 substrate in a 1 N H_2SO_4 solution at room temperature. The standard electrochemical cell was arranged to have a saturated Ag/AgCl electrode as the reference electrode and platinum as the counter electrode. The exposed area of the samples was 1.8 cm^2. The EIS measurements were carried out with Autolab PGSTAT 302N Potentiostat/Galvanostat and FRA2 frequency response analyzer at open circuit potential with the AC amplitude of 20 mV over a frequency range of 100 kHz to 1 MHz. Coating thickness was determined using the SEM image of the cross section of the coated sample.

3. Results and discussion

3.1. Thermal analysis

To achieve the best heat treatment temperature of the YSZ and to obtain the process pathways such as water or organic substance evaporation and phase transitions, the YSZ xerogel powder was subjected to thermal analysis (TG-DTA). It was first dried at 80 °C for 1.5 hours in an oven and then heated from room temperature to 800 °C in air atmosphere at a heating rate of 10 $°C.min^{-1}$. Figure 1 displays the TG/DTA results of the YSZ powder; it can be seen that weight loss stops at about 730 °C. The weight loss in the temperature range of 30 °C to 180 °C corresponds to the evaporation of superficial and structural water in the gel precursor. This is accompanied by two small endothermic peaks at 50 °C and 90 °C in the DTA curve respectively indicating the removal of superficial and structural water. As the temperature rises, two exothermic peaks accompanied by a sharp weight loss are observed between 180 °C and 480 °C. As shown in the TG curve, this sharp reduction of weight indicates that most of the organic species decompose in this range. Tiwari found that the weight loss during drying

sol-gel-derived yttria-doped zirconia powder by TG-DTA between 330 °C and 450 °C was due to the combustion of organic substances (Tiwari et al., 2009). The exothermic peak near 380 °C corresponds to the transition from amorphous to tetragonal phase of zirconia, which is confirmed by the XRD results. Soo found that the two exothermic DTA peaks of sol-gel derived powders near 350 °C and 421 °C corresponded to the decomposition of organic substances and the crystallization of tetragonal structure of zirconia respectively (Soo et al., 2012). The TG curve in the temperature range of 480 °C to 730 °C shows a slower rate of weight loss. Also, a wide exothermic peak from 550 °C to 725 °C can be seen in the DTA curve, which can be attributed to the growth of zirconia crystal size. This crystal growth is also approved by Scherrer equation in the XRD results. After a total weight loss of 47% up to 730 °C, the weight remains constant above 730 °C, which indicates the complete removal of organics.

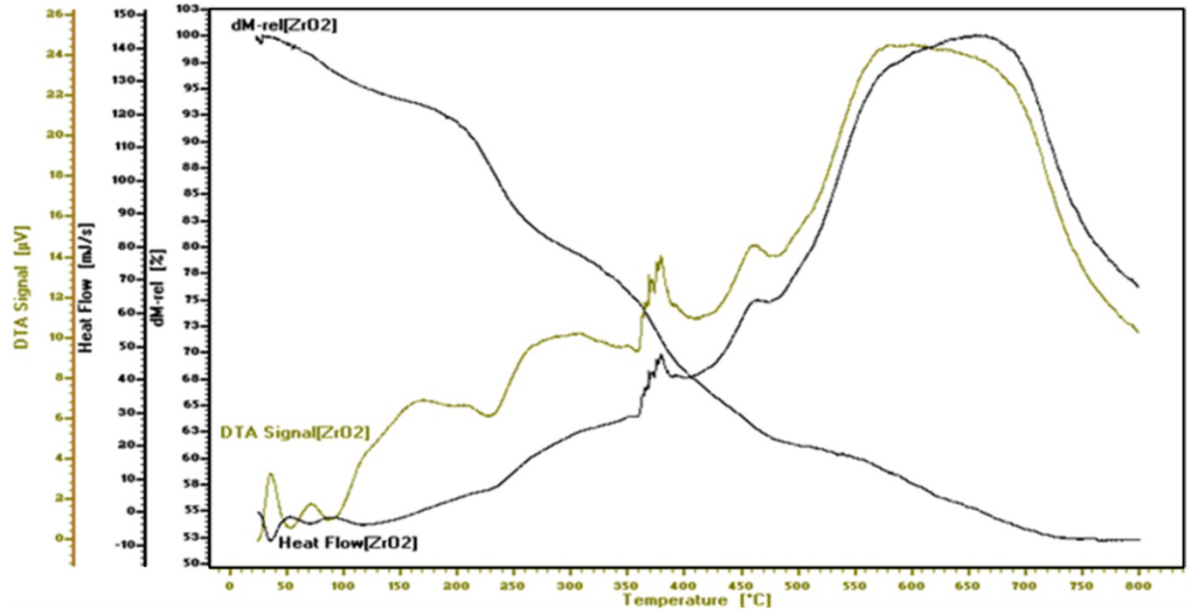

Figure 1
Thermal analysis (DTA-TG) curves of YSZ powder dried at 80 °C for 3 hrs in an oven

3.2. X-ray diffraction (XRD)

Figure 2 shows the XRD patterns of the gel powder after being thermally treated at three different temperatures of 150 °C, 400 °C, and 700 °C using a Bruker X-ray (D8ADVANCE, Germany; X-Ray tube anode: Cu, wavelength: 1.5406 Å(Cu K_α), filter: Ni); the analysis of the coating structure and coating formation process is done by using XRD patterns. The X-ray diffraction analyses indicate that the samples annealed at low temperatures about 150 °C are amorphous. When the powder is heat-treated at higher temperatures, the zirconia coatings are crystalline in the tetragonal phase, and the crystallinity increases with the temperature of the treatment. According to the patterns of Figure 2 (b), the crystallization of zirconia starts at temperatures near 400 °C , which is well matched with the previous works revealing the formation of crystallized yttria-stabilized zirconia above 575 K (Crespo et al., 2009; Fedrizzi et al., 2001; Nouri et al., 2011; Li et al., 2009). This can easily verify the attribution of the DTA exothermic peak near 380 °C to the crystallization of zirconia. The intensity of the XRD patterns of the YSZ thin films is weak and broadened near 400 °C. This may be ascribed to both the organic compounds remaining from the sol-gel process and small crystallite size (nanosize

effect). The crystal size D of the sample is measured using Scherrer equation (Crespo et al., 2009; Fedrizzi et al., 2001):

$$D_{hkl} = \frac{k\lambda}{B}\cos(\theta) \quad (1)$$

where, D_{hkl} denotes the average crystallite size of the synthesized YSZ; k is the shape factor and equal to 0.94; λ stands for the X-ray wavelength of Cu Kα and is equal to 0.15406 nm; B is the full width of the peak measured at half maximum intensity (FWHM) in radians and θ represents the Bragg's angle of the peak. The average crystalline size of the YSZ is 5.64 nm and 10.22 nm at the temperatures of 400 °C and 700 °C respectively, which approves the peak attributed to the crystal growth at temperatures between 550 °C and 725 °C in the DTA curve. It can also be seen that the amorphous to crystalline transformation from 150 °C to 400 °C is obvious. Also, the intensity of the peaks increases from 150 °C to 400 °C.

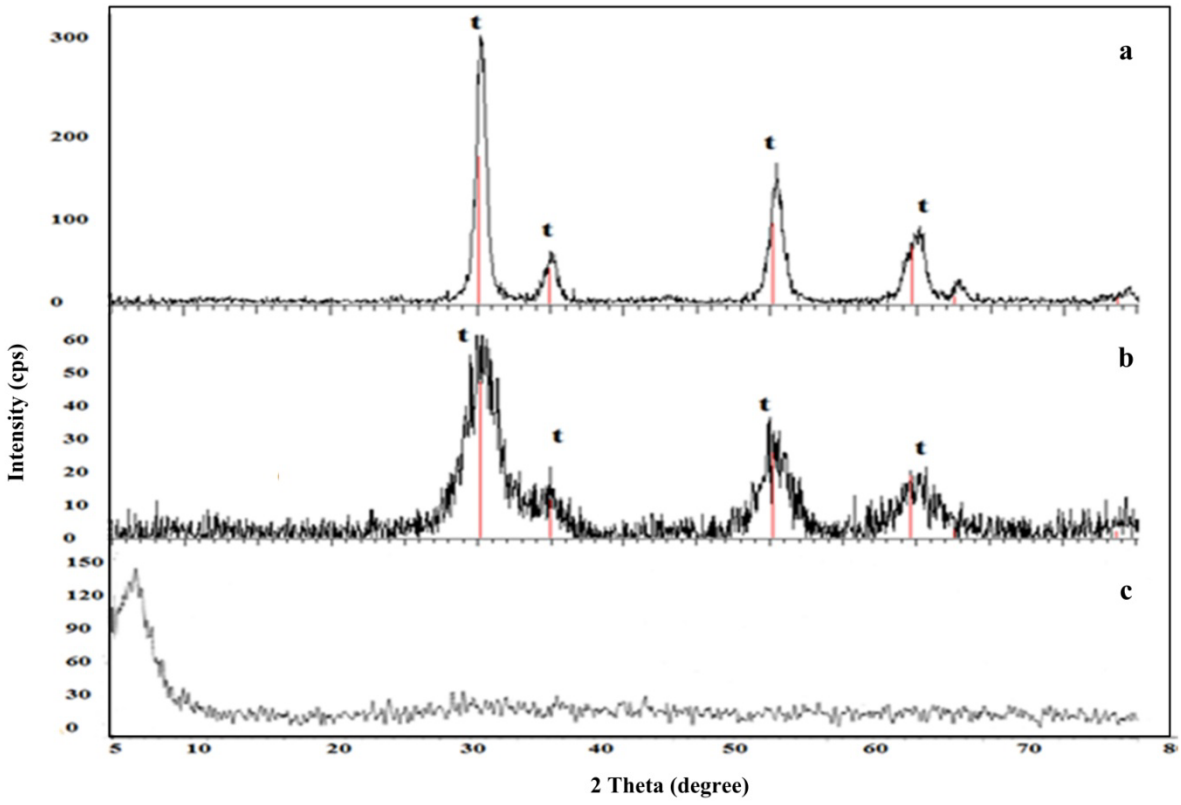

Figure 2
XRD spectra of the YSZ powders sintered at: (a) 150 °C; (b) 400 °C; and (c) 700 °C.

The critical crystalline size is 30 nm for pure zirconia (Xia et al., 2009). This parameter increases in the presence of yttria as a tetragonal stabilizer, and a higher temperature is required to reach a critical size so that the YSZ phase transforms to an undesirable monoclinic phase.

3.3. Energy dispersive x-ray (EDX)

Figure 3 shows the energy dispersive X-ray of the YSZ coated sample. The elemental composition of the YSZ coating determined by the EDX analysis is shown in Table 2. The weight percent of the yttrium is about 8 wt.% as it is expected.

Table 2
Elemental composition and weight percent of the YSZ coating

Element	Series	Unn. C (wt.%)	Norm. C (wt.%)	Atom. C (at.%)
Oxygen	K series	18.45	16.43	52.80
Yttrium	L series	7.22	6.43	3.72
Zirconium	L series	86.62	77.15	43.49

Total: 112.3%

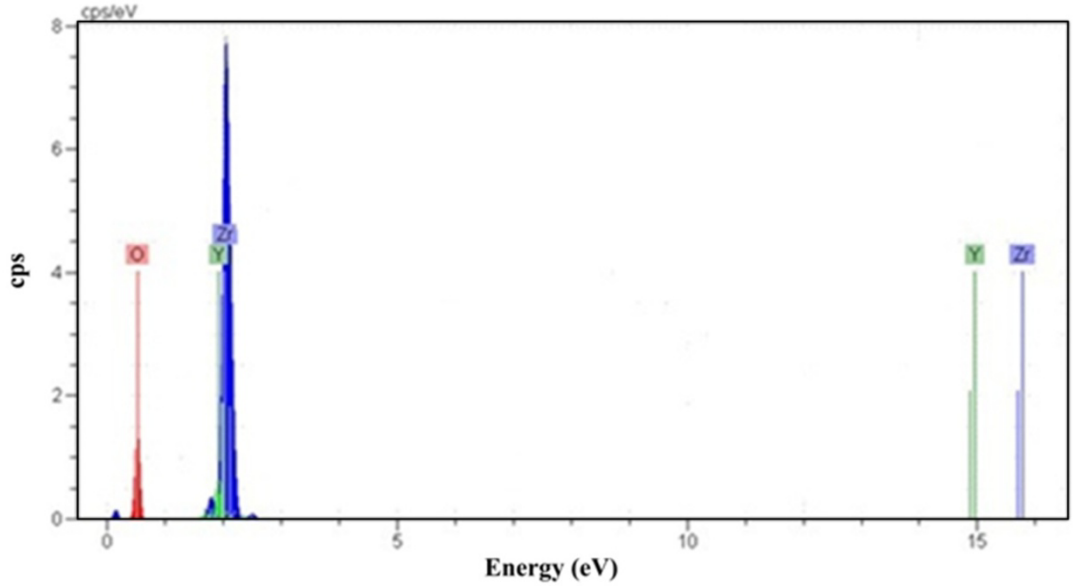

Figure 3
Energy dispersive X-ray spectroscopy (EDX) of the YSZ coating

3.4. Surface morphology

a. SEM characterization

The surface morphology of the YSZ thin films prepared using different molar ratios of water to alkoxide was displayed in Figure 4. As it is shown in Figures 4a-d, by increasing the molar ratio of water to alkoxide from 4 to 20, more cracks can be seen in the coatings. The more homogenous and uniform coverage of the surface corresponds to the water/alkoxide molar ratio equal to 4, and the cracks formed at a water/alkoxide molar ratio of 20 are more continuous than those created at a water/alkoxide molar ratio of 12. The extent of alkoxide hydrolysis, which depends on the amount of water, is one of the factors that can affect the densification behavior, which consequently causes the presence of stress and crack formation in the films (Sakka, 2004; Turova et al., 2002). At a water/alkoxide molar ratio of 1, the hydrolysis reaction is incomplete due to the inadequate amount of water; therefore, the proper coating with desirable properties is not formed. In the presence of excess water, there is a larger number of OH groups vulnerable to polycondensation reactions. This causes more polycondensation reactions to happen in the gel films during film drying over 100 °C. However, according to the works of Kozuka (Kozuka et al., 2004), the slope of the stress-temperature relation is similar irrespective of the water/alkoxide ratios at temperatures above 100 °C at which polycondensation reactions proceed. This implies that the occurrence of more polycondensation reactions is ruled out as the origin of a higher stress is observed at larger water/alkoxide ratios.

Lower water/alkoxide molar ratios could result in metalloxane polymers with a less branched structure. Such a structure promotes structural relaxation, leading to smaller rates of stress increasing during heating. Also, the capillary pressure, which is proportional to the surface tension of the vaporizing liquid, is higher at larger water/alkoxide molar ratios because water has much higher surface tension (72 $mN.m^{-1}$) relative to ethanol (22 $mN.m^{-1}$). The structural relaxation and lower capillary pressure is the reasons for the lower stress at lower water/alkoxide molar ratios. In the presence of a lower stress, denser and more crack-free films are formed (Sakka, 2004).

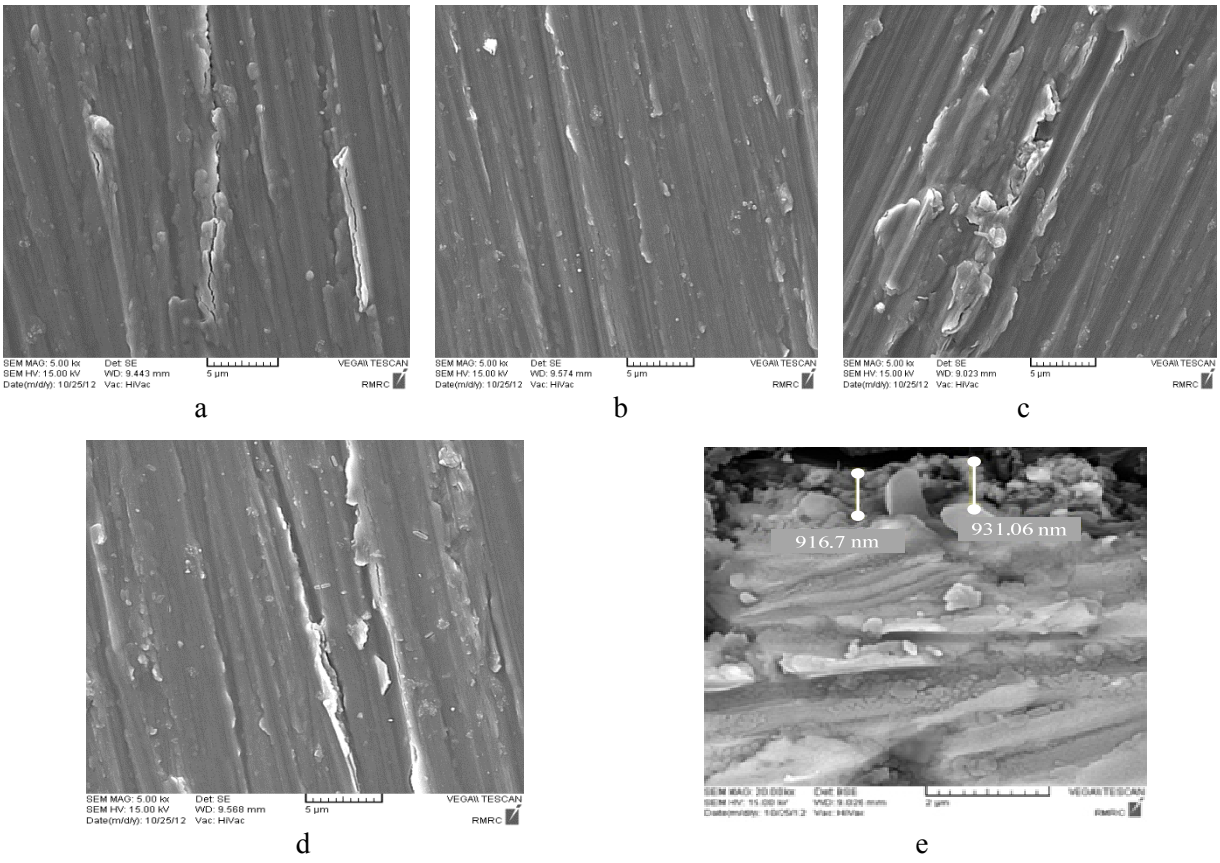

Figure 4
SEM images of the surface of the coated samples at different water/alkoxide molar ratios: (a) 1; (b) 4; (c) 12; (d) 20; and (e) the cross section of the YSZ coated sample

The film thickness of the coatings determined using the SEM image of the cross section of a 15-layer coating is displayed in Figure 4e. The total thickness of the coating after 15 deposited layers is about 900 nm; the thickness of each layer is about 60 nm.

3.5. Electrochemical measurements

a. Dynamic polarization

The YSZ coatings with different water/alkoxide molar ratios and heat-treated at 700 °C were coated on zircaloy-4 and examined in a 1 N H_2SO_4 electrolyte solution at 25 °C to study the influence of the water/alkoxide molar ratio on the quality and corrosion protection performance of the sol-gel derived YSZ dip coating. The parameters were obtained in the potential range of ±1.5 V from OCP. The polarization measurements were started after the attainment of a steady state under OCP conditions after about 30 minutes. Figure 5 shows the electrochemical polarization curves of the bare zircaloy-4 and the YSZ coated samples with different water/alkoxide molar ratios of 1, 4, 12, and 20. The

corrosion current density of the coated sample with a water/alkoxide molar ratio of 1 is decreased in comparison with the bare substrate due to the incomplete hydrolysis and polycondensation reactions in the case of insufficient amount of water. A critical amount of water is important for obtaining a transparent sol and a homogeneous coating as it was discussed in the microstructural studies. The corrosion potential, E_{corr}, of the other coated samples with water/alkoxide molar ratios higher than 1 is shifted to a more positive direction and the corrosion current density, i_{corr}, is decreased significantly compared with the bare substrate regardless of the water/alkoxide molar ratio. This observation approves the protective nature of the YSZ ceramic coatings against corrosion. As the water/alkoxide ratio increases up to 4, the protective ability of the coating is improved, while at higher ratios it is damaged because of the higher stress created at higher water/alkoxide molar ratios; this is due to a higher capillary pressure and more developed network structures, which produce more cracks and defects as discussed before. Although the possibility of interconnected cracks after a three-time deposition decreases, they cannot be removed completely.

Due to the presence of cracks and defects in the coating, the diffusion rate increases in terms of the increased current density (Crespo et al., 2009; Ruhi et al., 2009). In this manner, the morphology of the coated samples with higher water/alkoxide molar ratios reveals the presence of several cracks which may enhance the diffusion of the electrolyte through the coating at the metal/coating interface. On the contrary, the YSZ coated samples produced at lower water/alkoxide ratios show a denser microstructure and better barrier properties. As it is illustrated in Figure 5, the best corrosion protection, according to the polarization test, is obtained at a water/alkoxide molar ratio of 4 and reduces the corrosion current density by 3 orders of magnitude; it shifts the corrosion potential to a positive direction by more than 250 mV compared with the bare substrate. The corrosion potential shifts to a negative direction and the corrosion current density increases as the water/alkoxide molar ratio rises. Contrary to organic coatings that are permeable to water and oxygen, the sol-gel ceramic coatings act as a dielectric material and can only corrode through the defects and/or pinholes in the coating layer (Fedrizzi et al., 2001). Hence, the corrosion process takes place in flaws through which the electrolyte approaches the metallic substrate.

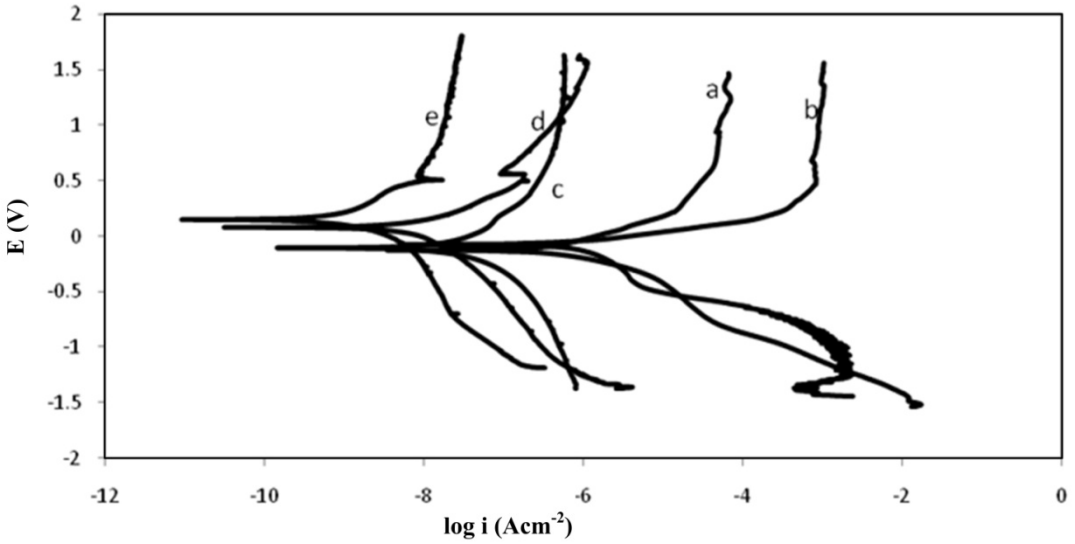

Figure 5
Potentiodynamic polarization curve measured in a 1 N H_2SO_4 solution for the bare and coated zircaloy-4: (a) bare; (b) water/alkoxide molar ratio of 1; (c) water/alkoxide molar ratio of 20; (d) water/alkoxide molar ratio of 12; and (e) water/alkoxide molar ratio of 4.

The corrosion current density is obtained from the intersection of anodic and cathodic Tafel lines. Table 3 tabulates the polarization resistance (R_p) values for the bare steel and the samples coated at different water/alkoxide molar ratios. The R_p values are found to decrease by increasing the water/alkoxide molar ratio. The maximum level of protection is achieved at a water/alkoxide molar ratio of 4 and is equal to $3.24\times10^{+6}$.

Table 3
Electrochemical parameters of potentiodynamic polarization curves calculated from the Tafel plots

Water/Alkoxide Ratio	i_{corr} (A.cm^{-2})	E_{corr} (V)	β_a (V.dec^{-1})	β_c (V.dec^{-1})	R_p (ohm.cm^2)	Corr. Rate (mm. yr^{-1})
Bare	5.01×10^{-8}	-0.126	0.037	0.044	$4.37\times10^{+3}$	5.880×10^{-4}
1	9.99×10^{-8}	-0.077	0.036	0.043	$3.82\times10^{+3}$	1.174×10^{-3}
4	9.35×10^{-11}	0.151	0.046	0.049	$3.24\times10^{+6}$	1.098×10^{-6}
12	6.19×10^{-10}	0.073	0.034	0.048	$6.30\times10^{+5}$	7.270×10^{-6}
20	1.60×10^{-9}	-0.105	0.041	0.036	$2.21\times10^{+3}$	1.879×10^{-5}

b. Electrochemical impedance spectroscopy (EIS)

Electrochemical impedance spectroscopy was carried out on the bare substrate and the sol-gel samples with different water/alkoxide molar ratios after having been immersed in a 1 N H_2SO_4 solution for 50 hours in order to evaluate their protective properties and corrosion mechanism. This is a powerful method for corroborating macroscopic behavior, corrosion, and electrochemical phenomena on metal samples coated by sol-gels (Crespo et al., 2009; Alvarez et al., 2010). Figure 6 shows the Nyquist plot of the bare and the coated samples. In a general manner, the impedance decreases as the water/alkoxide molar ratio rises to values larger than 1. This is due to the effect of the water/alkoxide molar ratio on the coating quality and crack formation as discussed above.

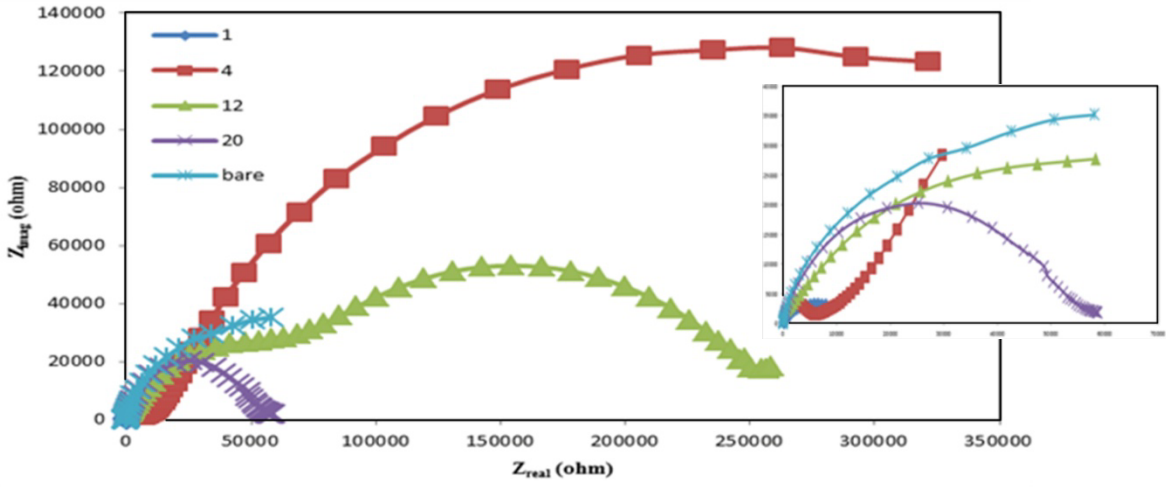

Figure 6
The Nyquist diagram of the bare and the coated samples after 50 hours

The sample with a water/alkoxide molar ratio of 4 shows the highest impedance over all frequency ranges during the immersion time, which indicates that this film provides the best barrier properties. Phase angle bode plot is also depicted in Figure 7.

In order to better explain the trend of the impedance diagrams, the electrochemical behavior is modeled using an equivalent electric circuit given in Figures 8a-b for the bare zircaloy-4 and the sol-

gel derived coatings. Figure 8b includes the models proposed by Andreatta (Andreatta et al., 2007) for a ZrO_2 pretreated AA6060 alloy and by Zheludkevich (Zheludkevich et al., 2006) for a hybrid coating pretreated AA2024-T3 alloy. Since the ceramic coatings are not permeable, the pores and cracks are the critical points which cause corrosion. The proposed model considers an outer layer containing large pores and an intermediate layer that might also contain defects (indicated as oxide) for 50 hours of immersion. Here, a constant phase element (CPE) is commonly used to represent capacitance. It is defined by the admittance (Y) and power index number (n) as follows:

$$Y = Y_0 (j\omega)^n \tag{2}$$

If n is equal to 0, resistive behavior will prevail, while if n is equal to 1, the capacitive behavior of the interface is encountered. Generally, ceramic treatments improve the corrosion resistance due to the formation of protective oxides that prevent oxygen and electrolyte from diffusing into the metal surface. R_s is the solution resistance; the constant phase element (CPE_{coat}) models the intact layer, while the resistance R_p is associated to large pores in the outer layer. The intermediate oxide is modeled with the constant phase element (CPE_{ox}) and the resistance R_{ox}. The mesh describing the substrate (CPE_{dl} and R_{ct}) is shown in the equivalent circuit in Figure 8. CPE_{ox} describes a network of electrolyte resistances and double layer capacitors in the pores of the layer, while R_{ox} is related to the barrier properties of the film. The parameter R_{ox} is affected by nano-pores in this layer. Therefore, this is the most important parameter of the equivalent circuit as long as corrosion protection is concerned. Table 4 displays the fitting parameters obtained for the YSZ pre-treated zircaloy-4 using the equivalent circuit in Figure 8. The behavior of the YSZ pre-treated zircaloy-4 strongly depends on the quality of the film formed on the alloy surface.

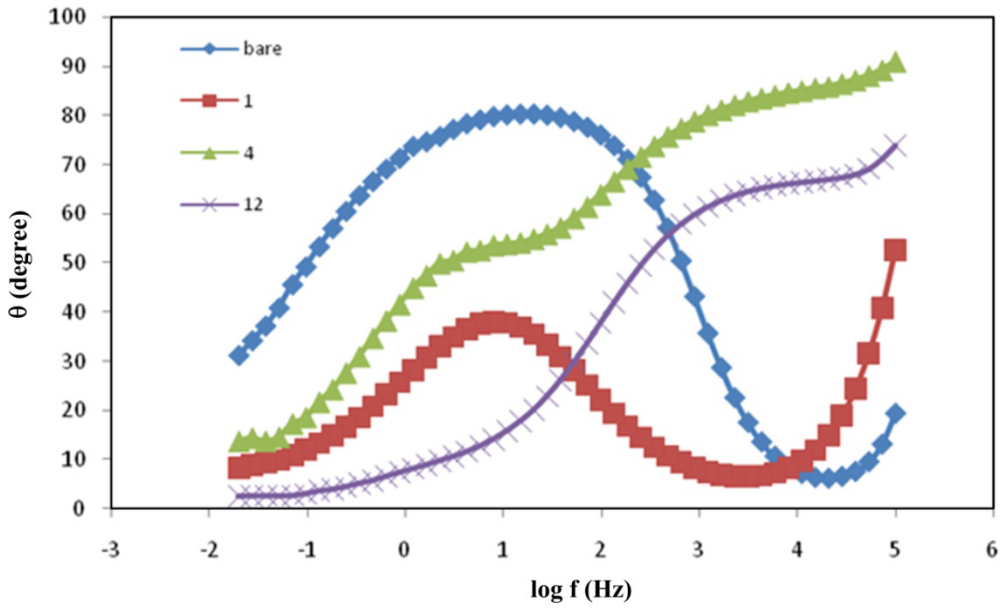

Figure 7
Bode plots of the YSZ coated samples after 50 hours

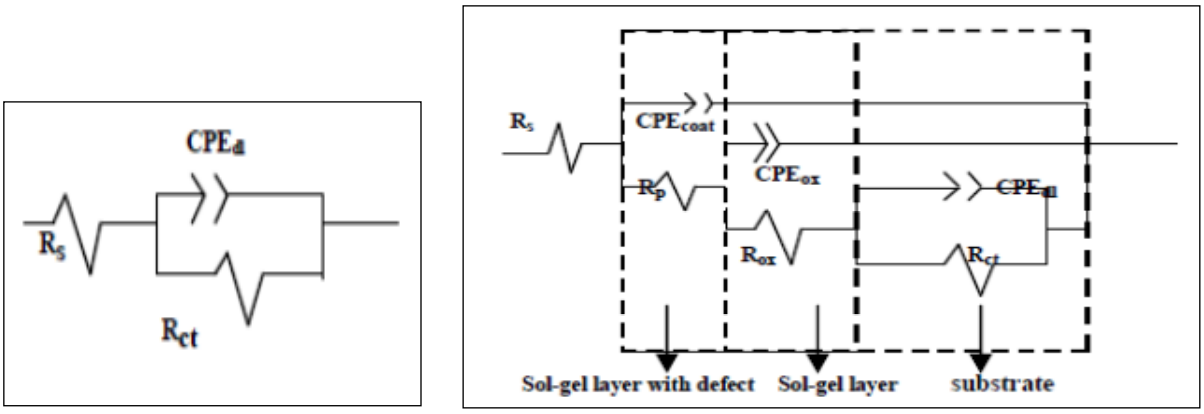

a b

Figure 8
Equivalent electric circuit of: (a) the bare and (b) the coated samples after 1-5 days of immersion

Table 4
EIS parameters corresponding to the equivalent circuit in Figure 8b

Electrode	R_S	CPE_{ox}		R_{ox}	CPE_{dl}		R_{ct}
	($\Omega.cm^2$)	Y_0(Fcm^2)	n	($\Omega.cm^2$)	Y_0(Fcm^2)	n	($\Omega.cm^2$)
Bare	12	----	----	----	3.31×10^{-5}	0.89	$7.22\times10^{+4}$
1	0.01	9.58×10^{-5}	0.49	266	2.30×10^{-4}	0.66	1.06×10^{-4}
4	0.01	2.22×10^{-10}	1.00	8634	6.40×10^{-6}	0.59	$6.48\times10^{+5}$
12	0.01	1.35×10^{-8}	0.94	8035	9.70×10^{-7}	0.56	$1.87\times10^{+5}$
20	0.01	2.40×10^{-4}	0.80	3248	4.27×10^{-13}	0.31	485

The present EIS results are in good agreement with the corrosion rate measured by the Tafel plots and accord with the microstructural studies.

4. Conclusions

The present work reveals that controlling the sintering temperature allows the formation of crystalline YSZ thin films, which can consequently offer a suitable response as protective barriers. This is due to the organic substance evaporation. The crystallinity rises by increasing temperature. Also, in the hydrolysis reactions, the amount of water is an essential parameter for a successful process. In the case of an insufficient amount of water, the hydrolysis reaction is not complete. Moreover, in the presence of a large amount of water, the coating quality is damaged. The water/alkoxide molar ratio has a great influence on the quality and corrosion resistance of the sol-gel derived YSZ coatings. This ratio changes the surface morphology of the coatings. The SEM images show that crack-free coatings are obtained at lower water/alkoxide molar ratios, and higher water/alkoxide molar ratios causes a cracked appearance. This fact can explain the worst behavior of the samples produced at larger water/alkoxide molar ratios in Tafel test. Furthermore, the impedance measurements are in good agreement with the Tafel test. The best corrosion resistance corresponds to a water/alkoxide molar ratio of 4. The observed behavior is related to the structural relaxation and a lower capillary pressure, which are both created at lower water/alkoxide molar ratios; additionally, a lower water/alkoxide molar ratio results in a lower stress.

Nomenclature

°C	: Degree Centigrade
μm	: Micrometer
s	: Second
mm	: Millimeter
N	: Normality
wt.%	: Weight Percent

References

Alvarez, P., Collazo, A., Covelo, A., Novoa, X.R., Perez, C., The Electrochemical Behavior of Sol-gel Hybrid Coatings Applied on AA2024-T3 Alloy: Effect of the Metallic Surface Treatment, Progress in Organic Coatings, Vol. 69, p. 175-183, 2010.

Andreatta, F., Aldighieri, P., Paussa, L., Maggio, R.D., Rossi, S., Fedrizzi, L., Electrochemical Behavior of ZrO_2 Sol-gel Pre-treatments on AA6060 Aluminum Alloy, Electrochimica Acta, Vol. 52, p. 7545-7555, 2007.

Baron, Y.S., and Ruiz, A., Sol-gel Coating to Reduce 1.25Cr-0.5Mo Steel Oxidation at 700 °C: Catalyst Type Effect, Corrosion Science, Vol. 53, p. 1060-1065, 2011.

Carrion, R.U., Sittner, F., Yekehtaz, M., Flege, S., Brotz, J., Ensinger, W., Influence of Stabilizing Agents on Structure and Protection Performance of Zirconium Oxide Films, Surface & Coatings Technology, Vol. 204, p. 2064-2067, 2010.

Carrion, R.U., Sittner, F., Ochs, C.J., Flege, S., Ensinger, W., Characterization of the Porosity of Thin Zirconium Oxide Coatings Prepared at Low Temperatures, Thin Solid Films, Vol. 517, p. 1967-1969, 2009.

Chen, Y., Macdonald, M. U., Macdonald, D. D., The Electrochemistry of Zirconium in Aqueous Solutions at Elevated Temperatures and Pressures, Journal of Nuclear Materials, Vol. 348, p. 133-147, 2006.

Crespo, M.A.D., Murillo, A.G., Huerta, A.M.T., Romo, F.J.C., Bustamante, E.O., Zamora, C.Y., Characterization of Ceramic Sol-gel Coatings as an Alternative Chemical Conversion Treatment on Commercial Carbon Steel, Electrochimica Acta, Vol. 54, p. 2932-2940, 2009.

Fedrizzi, L., Rodriguez, F. J., Rossi, S., Deflorian, F., Maggio, R. D., The Use of Electrochemical Techniques to Study the Corrosion Behavior of Organic Coatings on Steel Pretreated with Sol-gel Zirconia Films, Electrochimica Acta, Vol. 46, p. 3715-3724, 2001.

Jokinen, M., Patsi, M., Rahiala, H., Peltola, T., Ritala, M., Rosenholm, J.B., Influence of Sol and Surface Properties on In Vitro Bioactivity of Sol-gel-derived TiO_2 and TiO_2-SiO_2 Films Deposited by Dip-coating Method, John Wiley & Sons, Inc., Vol. 98, p. 295-298, 1998.

Kim, H. H., Kim, J. H., Moon, J. Y., Lee, H. S., Kim, J. J., Chai, Y. S., High-temperature Oxidation Behavior of Zircaloy-4 and Zirlo in Steam Ambient, J. Mater. Sci. Technol., Vol. 26, p. 827-832, 2010.

Kiruthika, P., Subasri, R., Jyothirmayi, A., Sarvani, K., Hebalkar, N.Y., Effect of Plasma Surface Treatment on Mechanical and Corrosion Protection Properties of UV-curable Sol-gel Based GPTS-ZrO_2 Coatings on Mild Steel, Surface & Coatings Technology, Vol. 204, p. 1270-1276, 2010.

Kozka, H., and Komeda, M., Effect of the Amount of Water for Hydrolysis on Cracking and Stress Evolution in Alkoxide-derived Sol-gel Silica Coating Films, Japan, Journal of the Ceramic Society of Japan, Vol. 112, p. s223-s227, 2004.

Li, H., Liang, K., Mei, L., Gu, S., Wang, S., Oxidation Protection of Mild Steel by Zirconia Sol-gel

Coatings, Materials Letters, Vol. 51, p. 320-324, 2001.

Li, Q., Zhong, X., Hu, J., Kang, W., Preparation and Corrosion Resistance Studies of Zirconia Coating on Fluorinated AZ91D Magnesium Alloy, Progress in Organic Coatings, Vol. 63, p. 222-227, 2008.

Li, Q., Chen, B., Xu, S., Gao, H., Zhang, L., Liu, C., Structural and Electrochemical Behavior of Sol-gel ZrO_2 Ceramic Film on Chemically Pre-treated AZ91D Magnesium Alloy, Journal of Alloys and Compounds, Vol. 478, p. 544-549, 2009.

Lopez, A.J., Rams, J., Urena, A., Sol–gel Coatings of Low Sintering Temperature for Corrosion Protection of ZE41magnesium Alloy, Surface & Coatings Technology, Vol. 205, p. 4183-4191, 2011.

Liu, W., Chen, Y., Ye, Ch., Zhang, P., Preparation and Characterization of Doped Sol-gel Zirconia Films, Ceramics International, Vol. 28, p. 349-354, 2002.

Neto, P.D. L., Atik, M., Avaca, L.A., Aegerter, M.A., Sol-gel Coatings for Chemical Protection of Stainless Steel, Journal of Sol-Gel Science and Technology, Vol. 2, p. 529-534, 1994.

Nouri, E., Shahmiri, M., Rezaie, H.R., Talayian, F., A Comparative Study of Heat Treatment Temperature Influence on the Thickness of Zirconia Sol-gel Thin Films by Three Different Techniques: SWE, SEM and AFM, Surface & Coatings Technology, Vol. 206, p. 3809-3815, 2012.

Nouri, E., Shahmiri, M., Rezaie, H.R., Talayian, F., Investigation of Structural Evolution and Electrochemical Behavior of Zirconia Thin Films on the 316L Stainless Steel Substrate Formed via Sol-gel Process, Surface & Coatings Technology, Vol. 205, p. 5109-5115, 2011.

Paussa, L., Rosero Navarro, N.C., Bravin, D., Andreatta, F., Lanzutti, A., Aparicio, M., Duran, A., Fedrizzi, L., ZrO_2 Sol-gel Pre-treatments Doped with Cerium Nitrate for the Corrosion Protection of AA6060, Progress in Organic Coatings, Vol. 74, p. 311-319, 2012.

Peng, D.Q., Bai, X.D., Chen, B.S., Surface Analysis and Corrosion Behavior of Zirconium Samples Implanted with Yttrium and Lanthanum, Surface & Coatings Technology, Vol. 190, p. 440-447, 2005.

Peng, D.Q., Bai, X.D., Chen, X.W., Zhou, Q.G., Liu, X.Y., Yu, R.H., Deng, P.Y., Corrosion Behavior of Tin Ions Implanted Zirconium in 1 N H_2SO_4, Applied Surface Science, Vol. 239, p. 342-352, 2005.

Peng, D.Q., Bai, X.D., Chen, W., Zhou, Q.G., Liu, X.Y., Yu, R.H., Corrosion Behavior in 1 N H_2SO_4 Solution of Zirconium Ion Implanted with Nickel, Vol. 187, p. 300-306, 2004.

Peng, D.Q., Bai, X.D., Chen, X.W., Zhou, Q.G., Liu, X.Y., Deng, P.Y., Comparison of Aqueous Corrosion Behavior of Zirconium and Zircaloy-4 Implanted with Molybdenum, Nuclear Instruments and Methods in Physics Research B, Vol. 211, p. 55-68, 2003.

Ruhi, G., Modi, O.P., Singh, I.B., Pitting of AISI 304L Stainless Steel Coated with Nano-structured Sol-gel Alumina Coatings in Chloride Containing Acidic Environments, Corrosion Science, Vol. 51, p. 3057-3063, 2009.

Sakka, S., Handbook of Sol–gel Science and Technology, Processing, Characterization and Applications, Vol. 1, 688 P. Kluwer Academic Publishers, 2004.

Sanchez, A. G., Schreiner, W., Duffo, G., Cerea, S., Surface Characterization of Anodized Zirconium for Biomedical Applications, Applied Surface Science, Vol. 257, p. 6397-6405, 2011.

Soo, M.T., Prastomo, N., Matsuda, A., Kawamura, G., Muto, H., Fauzi Mohd Noor, A., Lockman, Z., Cheong, K.Y., Elaboration and Characterization of Sol-gel Derived ZrO_2 Thin Films Treated with Hot Water, Applied Surface Science, Vol. 258, p. 5250-5258, 2012.

Shoesmith, D.W., and Zagidulin, D., The Corrosion of Zirconium under Deep Geologic Repository

Conditions, Journal of Nuclear Materials, Vol. 418, p. 292-306, 2011.

Stojilovic, N., Bender, E. T., Ramsier, R.D., Surface Chemistry of Zirconium, Progress in Surface Science, Vol. 78, p. 101-184, 2005.

Tiwari, S. K., Adhikary, J., Singh, T.B., Singh, R., Preparation and Characterization of Sol-gel Derived Yttria-doped Zirconia Coatings on AISI 316L, Thin Solid Films, Vol. 517, p. 4502-4508, 2009.

Turova, N.Y., Turevskaya, E. P., Kessler, V.G., Yanovskaya, M.I., The Chemistry of Metal Alkoxides, Kluwer Academic Publishers, 573 p., 2002.

Voevodin, N. N., Grebasch, N. T., Soto, W.S., Kasten, L.S., Grant, J.T., Arnold, F.E., Donley, M.S., An Organically Modified Zirconate Film as a Corrosion-resistant Treatment for Aluminum 2024-T3, Progress in Organic Coatings, Vol. 41, p. 287-293, 2001.

Xia, X., Zhitomirsky, I., McDermid, J. R., Electrodeposition of Zinc and Composite Zinc-Yttria Stabilized Zirconia Coatings, Journal of Materials Processing Technology, Vol. 209, p. 2632-2640, 2009.

Xue, W., Zhu, Q., Jin, Q., Hua, M., Characterization of Ceramic Coatings Fabricated on Zirconium Alloy by Plasma Electrolytic Oxidation in Silicate Electrolyte, Materials Chemistry and Physics, Vol. 120, p. 656-660, 2010.

Zheludkevich, M. L., Serra, R., Montemor, M. F., Miranda Salvado, I.M., Ferreira, M.G.S., Corrosion Protective Properties of Nano-structured Sol-gel Hybrid Coatings to AA2024-T3, Surface & Coatings Technology, Vol. 200, p. 3084-3094, 2006.

Zhen-lin, W., and Rong-chang, Z., Comparison in Characterization of Composite and Sol-gel Coating on AZ31 Magnesium Alloy, Trans. Nonferrous Met. Soc. China, Vol. 20, p. 665-669, 2010.